Chapter 4

Dynamic shear strength of soil under cyclic torsional shear loading

4.1 Introduction

Soil failure during the operation of a tractor in the field brings about large soil deformation that results in the enormous deterioration and degradation of agricultural soil. A simple example of soil failure is the one that occurs beneath a driven lugged tire at the maximum tire traction force[57]. If the large deformation occurs during field operation, successive passes of the tractor will produce a severe level of soil compaction. It occurs excessively in the arable layer and its compacted zone might be deeper. Besides, not only the extreme soil compaction but also the reduction in trafficability of soil and tractive efficiency of a tractor has to be considered. Correspondingly, it will develop numerous adverse effects such as more power requirements for traction and air pollution by more CO_2 exhaust.

Taking into consideration the above serious problem, the test experiments were intended to perform investigation on the dynamic shear strength of soil being subjected to cyclic torsional shear loading. This study also focused on traffic-induced soil behavior, especially on torsional shear loading phenomena; quick turning, driving on irregular profile, operating on hillside. The interrelationships among the factors involved that were investigated in Chapter 3 served as a basic information of this soil when it is subjected to cyclic torsional shear load. The experimental design was, then, carried out. The results were analyzed and discussed in relation to shear strength and critical state theory.

4.2 Methodology

The soil specimen whose its physical properties were described in Chapter 3 was used in this experiment. In addition, the mechanical properties of this soil were prepared in order to serve as basic shear strength properties in comparison with the results of the cyclic torsional shear loading test. These soil properties were investigated by employing the conventional triaxial test. The results are shown in Figs. 4.1, 4.2 and 4.3, which represent intrinsic traits in terms of the effective shear strength, critical state line and failure characteristics, respectively. The soil specimens were prepared along with pre-set values, including moisture content of 25%d.b. and bulk densities of 1.0 Mg/m^3, and then used for the experiments under saturated, undrained conditions.

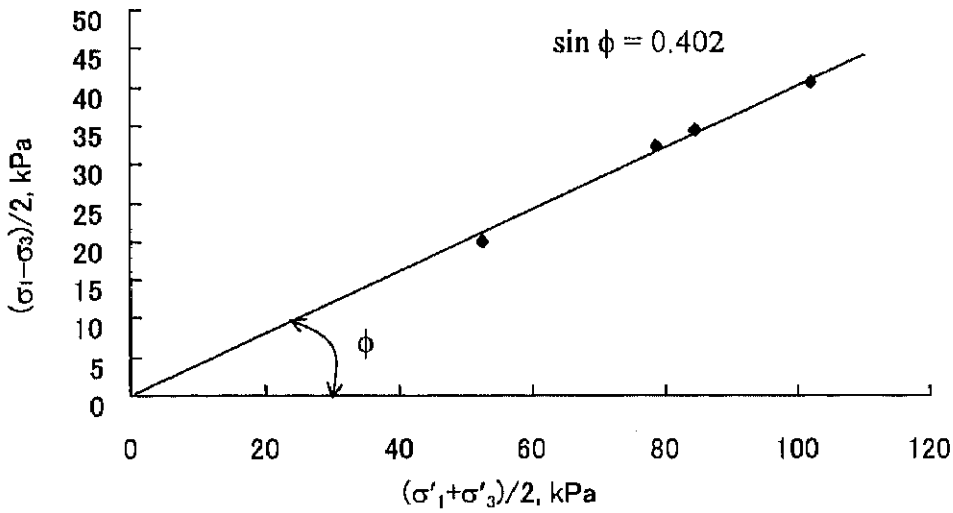

Fig. 4.1 Effective shear strength.

The ϕ presented in Fig. 4.1 was an angle of internal friction, which was equal to 23.7 deg. After being calculated directly from the parameters listed in the figure, the effective shear strength could be represented as $\tau = 0.44\sigma'_n$. For comparative purposes, the expression term of σ'_m was provided as follows:

$$\tau = 0.43\sigma'_m \tag{4.1}$$

The stress path in Fig. 4.2 exhibits the contractive behavior of soil that normally appeared under saturated, undrained conditions of a loose specimen. Accordingly, the critical state line can be established by the stress paths and formulated by the equation of

$$(\sigma'_1-\sigma'_3)/2 = 0.64\sigma'_m \tag{4.2}$$

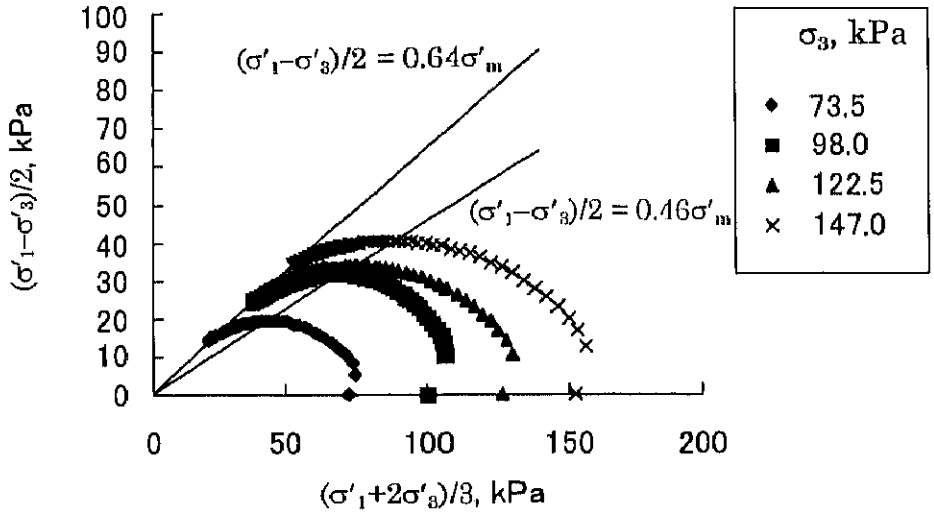

Fig. 4.2 Stress paths and critical state line.

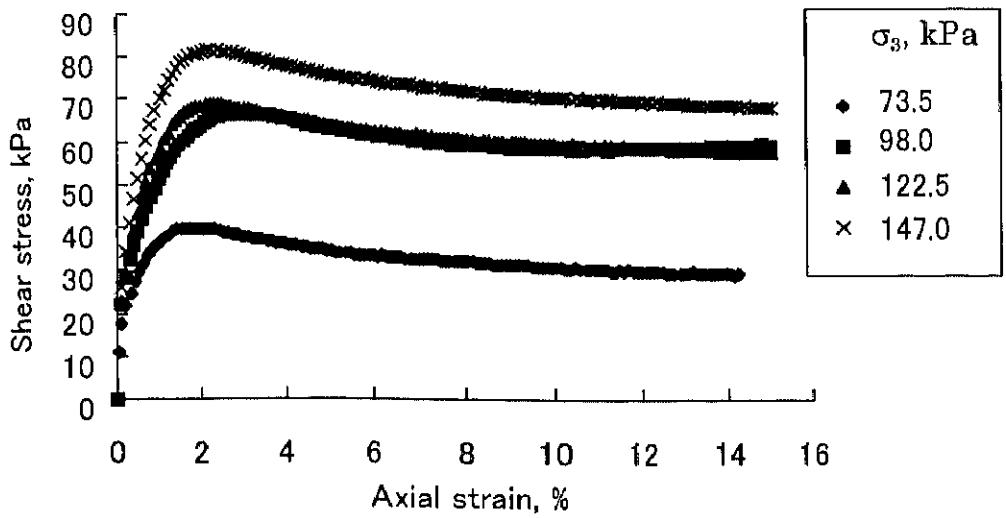

Fig. 4.3 Stress and strain relationship.

The relationship at maximum shear stress can be expressed by $(\sigma'_1-\sigma'_3)/2 = 0.46\sigma'_m$. Furthermore, the relationship between shear stress and axial strain in Fig. 4.3 was recognized as the strain softening with slight difference between the values of peak stress and residual stress.

For the cyclic torsional shear loading test, the specimen preparation and test procedure were the same as described in Chapter 3; but the loading process was continued until the specimen reached failure and the data related to failure characteristic were emphasized.

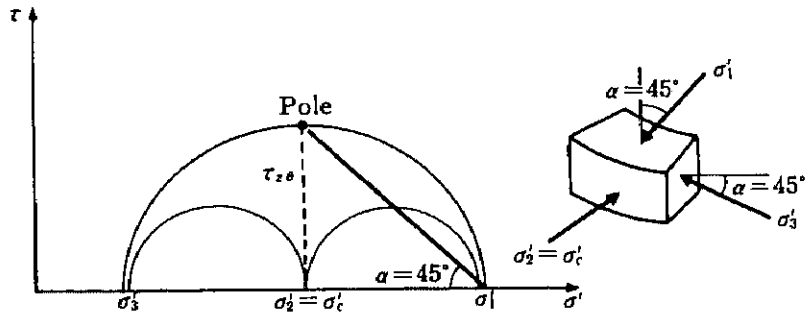

Fig. 4.4 Mohr's circle and principal stress directions.

The effective principal stresses that appeared in the soil specimen under this cyclic torsional shear loading mode can be expressed by the following equations:

$$\sigma'_1 = \sigma'_c + \tau_{z\theta} \tag{4.3}$$

$$\sigma'_2 = \sigma'_c \tag{4.4}$$

$$\sigma'_3 = \sigma'_c - \tau_{z\theta} \tag{4.5}$$

Morh's circles for these stresses can be drawn and the directions of principal stresses can be expressed in Fig. 4.4. σ'_m under this test condition was equivalent to σ'_c. σ'_m is to be evaluated by $(\sigma'_1+\sigma'_2+\sigma'_3)/3$. Substituting equations (4.3), (4.4) and (4.5) for σ'_m, the relation $\sigma'_m = \sigma'_c$ can be obtained. The test combinations are listed in Table 4.1. Parameters

involved on dynamic shear strength were to be investigated including torsional shear stress, torsional shear strain, pore water pressure, confining stress, loading frequency, bulk density and number of cyclic loading.

Table 4.1 Test combinations

Test No.	Bulk density, Mg/m^3	Frequency, Hz	Confining stress, kPa	Cyclic torsional shear stress, kPa
1	1.04	0.2	98.0	10.8
2	1.03	0.2	98.0	12.9
3	1.02	0.2	98.0	15.0
4	1.01	0.2	98.0	17.1
5	0.99	0.2	98.0	19.3
6	1.01	0.2	98.0	20.6
7	1.01	0.2	98.0	21.7
8	0.99	0.2	98.0	23.3
9	1.04	0.5	98.0	14.8
10	0.99	0.5	98.0	16.9
11	0.99	0.5	98.0	17.6
12	1.00	0.5	98.0	18.3
13	1.00	0.5	98.0	19.3
14	0.98	1.0	98.0	16.5
15	0.99	0.2	83.3	14.9
16	0.99	0.2	147.0	27.8
17	0.91	0.2	98.0	17.6
18	0.90	0.2	98.0	19.3
19	0.83	0.2	98.0	16.8
20	0.83	0.2	73.5	10.8

4.3 Results and discussion

4.3.1 Failure characteristics of soil

As described in Chapter 3, the strain softening behavior of a soil specimen was recognized after the constant cyclic torque was applied for a certain cycle. At this point, torsional shear stress started to decrease accompanied by a comparatively large increase of torsional shear strain and pore water pressure. In agricultural engineering, the point where the stress starts to decrease is significant for determination of the trafficability of soil and the tractive efficiency of a tractor. Hence, this point should be defined as a failure point of a soil specimen in this study. It may be different from the definition of the pertinent failure in the field of civil engineering. Besides, it should also be noted here that this test was a torque control not an actual stress control test. If a stress control test were conducted, the failure point might have been different. The amplitude of stress would be kept constant for a longer period. However, the torque control test seems to be more appropriate for the study of traffic-induced field soil compaction.

Again, the failure characteristic of soil under this case can be specified by strain softening phenomena without the initial liquefaction, but pore water pressure developed up to about 30% of the confining stress. Fig. 4.5 shows a typical corresponding stress path in terms of cyclic torsional shear stress and effective confining stress. With the increase of Nc during tests, the magnitude of torsional shear stress was kept constant while the effective confining stress was diminishing. During moving forward to the zero stress state, the amplitude of the torsional shear stress started to decrease at point-A and continued with slight decrease in the amount of torsional shear stress. This failure pattern is explicitly different from one where initial liquefaction is developed, as shown in Fig. 4.6. The stress path in Fig. 4.6 was suddenly triggered to zero stress state after tracing with constant shear

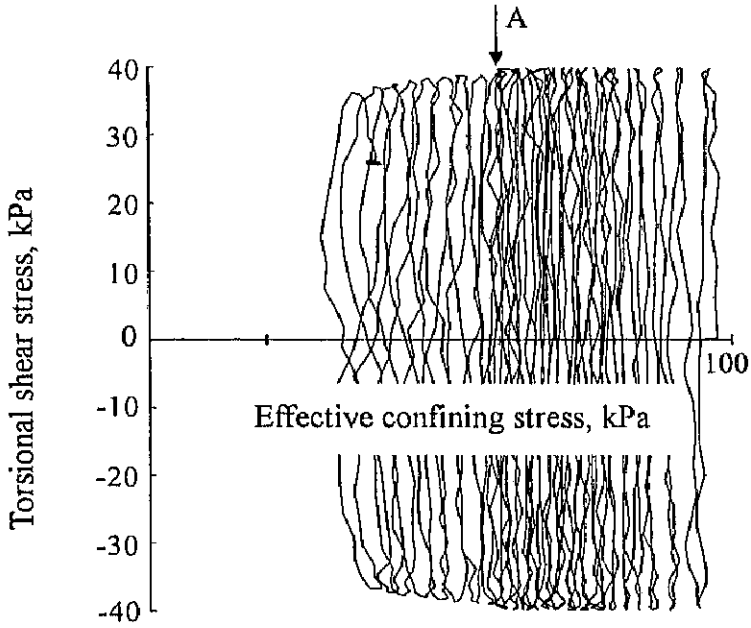

Fig. 4.5 Stress path for cyclic torsional shear loading.

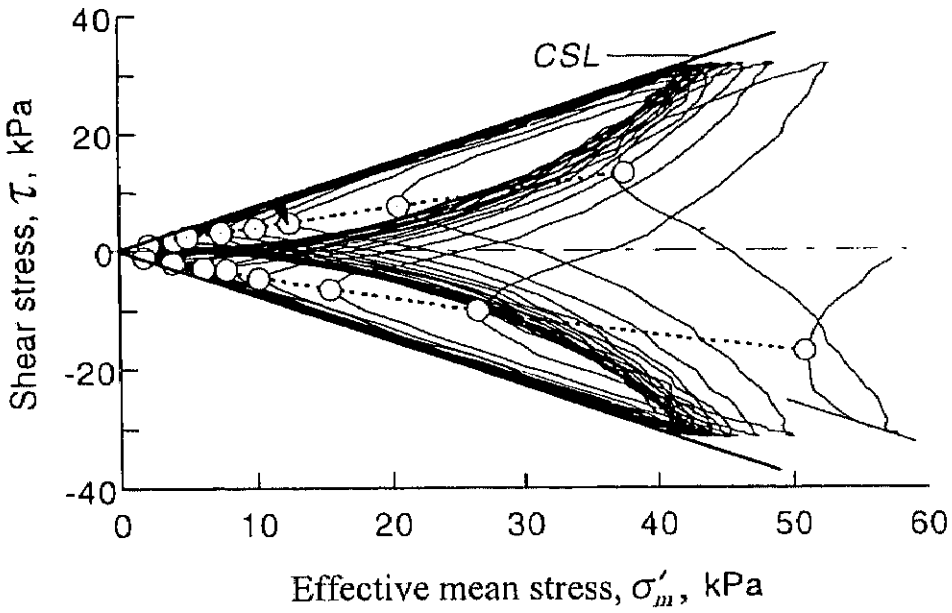

Fig. 4.6 Effective stress path of cyclic undrained shear test for Toyoura sand and $Dr = 96\%$ (After Zang *et al.*, 1997).

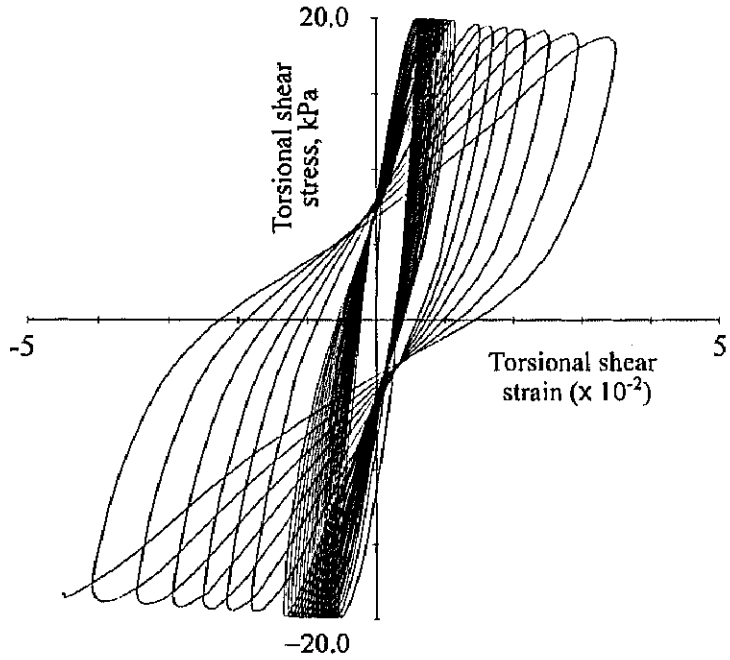

Fig. 4.7 Hysteresis loop of torsional shear stress and strain.

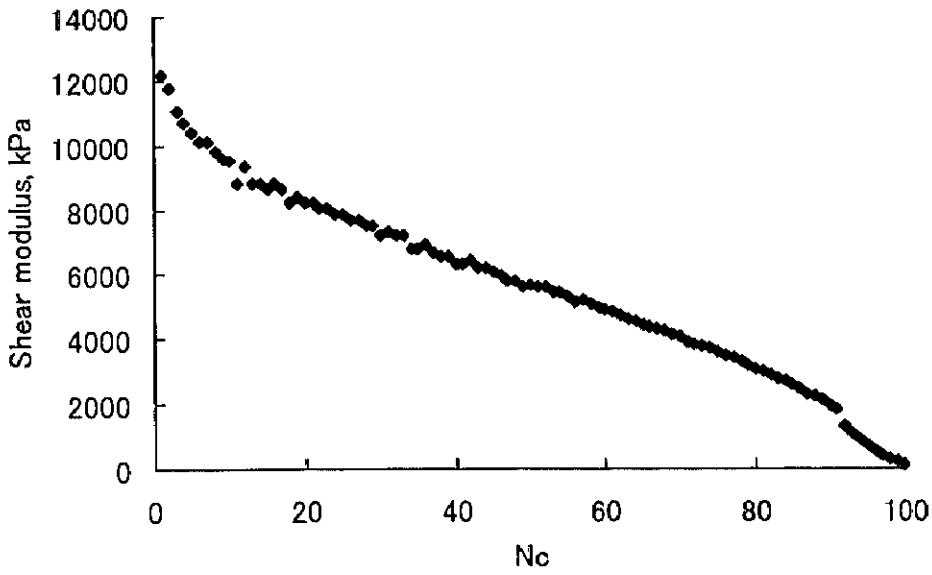

Fig. 4.8 Shear modulus versus Nc.

stress up to a certain number of loading. The physical properties, especially the percentage of finer particles of test soils, was considered a main cause of the difference. Note that soil in Fig. 4.6 was sand.

Fig. 4.7 shows the hysteresis loop under this test which tended to expand along the abscissa. Expansion of the hysteresis loop might imply the decrease of shear modulus of the soil. After failure, the shape of the hysteresis loop was changed following a sigmoid curve with a slight decrease of stress, indicating the strain softening phenomena.

The relationship of shear modulus and Nc during test can be observed in Fig 4.8. This is typical of the other test results obtained in this study. The shear modulus was reduced accompanying the increase of Nc. It is interesting that the shear modulus was inversely proportional to Nc starting at about Nc = 15 until soil failure. This relation might be useful in predicting the strength property of soil during cyclic loading application. In addition, it was manifested that soil was stretched at the initial stage, which can be observed by the relatively steeper slope of the initial tangent. This phenomenon seems to appear owing to the rearrangement of soil particles.

4.3.2 Dynamic shear strength behavior

In the study of cyclic loading for earthquake phenomena, the failure of soil is defined by the large development of soil deformation; for example, 20%[16] of strain for sand in normal cases and 5%[41] or 10%[40] for clay depending on test conditions. However, in soil-wheel interaction, even a small change in the soil's physical properties might show serious impact. On the one hand, the tractive efficiency is reduced. Considering that the maximum traction occurs at the maximum shear strength of soil at a certain level of slip, and after the soil fails, the high slip appears resulting in the reduction of tractive efficiency. On the other hand, serious soil deformation and compaction, in turn, is produced by high

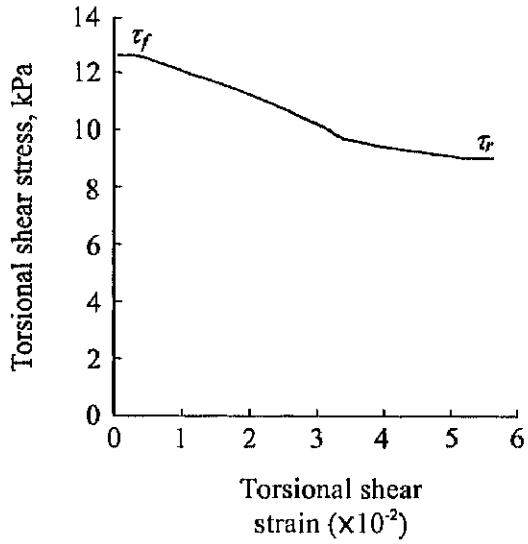

Fig. 4.9 Torsional shear stress and torsional shear strain.

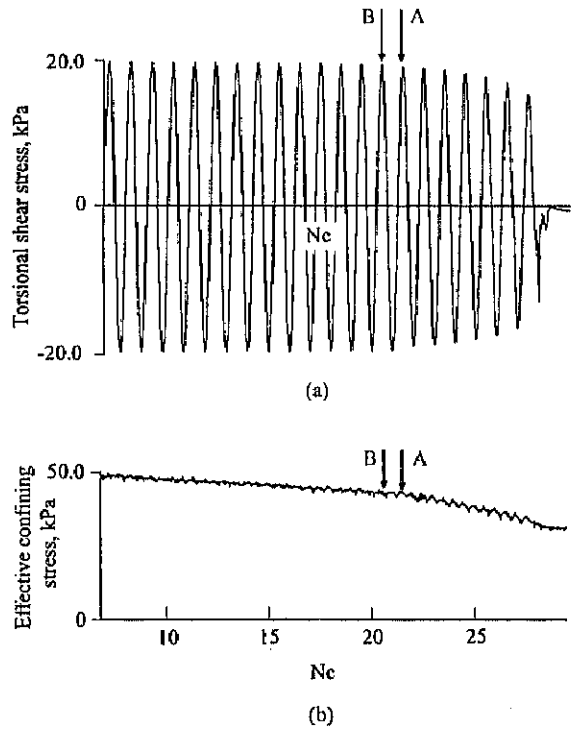

Fig. 4.10 (a) Torsional shear stress and
(b) effective confining stress versus Nc.

slip. Also the compacted zone might occur deeper, especially after successive wheel passes. Taking this into consideration, the determination of field soil failure should be related to the critical value of the stress rather than development of the strain. Therefore, dynamic failure in this specific study was defined based on the maximum shear stress criteria of the classical shear strength theory.

The shear strength is normally determined at the maximum stress state that the soil specimen can endure. Fig. 4.9 presents the stress-strain relationship in terms of amplitudes of torsional shear stress and strain at each loading cycle. It was seen that the peak value of shear stress, τ_f, can be observed before failure and residual stress, τ_r, appeared. The last cycle that contained τ_f was taken into account for determining dynamic shear strength. In order to easily specify the values of relevant shear strength parameters, the cyclic torsional shear stress and effective confining stress showing in relation with Nc were provided in Fig. 4.10. As presented before, the amplitude of the shear stress started to decrease on cycle-A, indicating failure state. Therefore, the previous cycle-B was chosen as the last cycle of constant loading amplitude that the specimen was able to support. Practically, the cycle-A and -B were determined by judging the change of relationship between the double amplitude of torsional shear stress and log Nc (Fig. 4.11). As shown in the figure, the relationship between the double amplitude of torsional shear stress and log Nc is more obviously distinguished between the cycle-A and -B when compared to the one in Fig.4.10(a). The shear strength parameters were determined by the amplitudes of torsional shear stress and the effective confining stress at the end of the cycle-B.

Applying the values of shear strength parameters to equations (4.3) and (4.5), σ_1' and σ_3' were obtained. Mohr circles for cyclic torsional shear strength, then, can be drawn as presented in Figs. 4.12, 4.13 and 4.14. These figures provided dynamic shear strength in

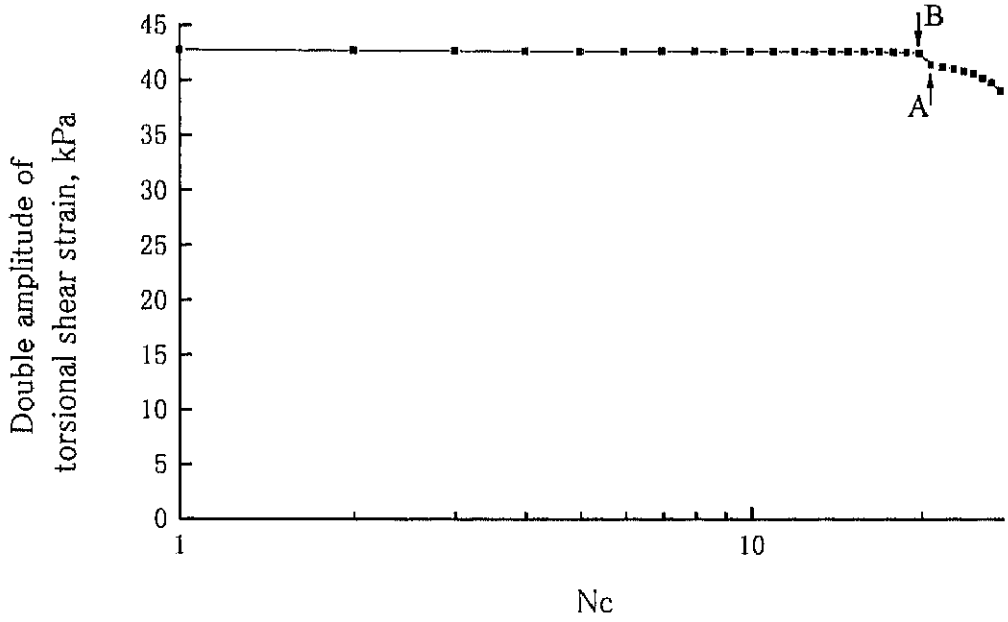

Fig. 4.11 Double amplitude of torsional shear stress versus Nc.

different test combinations in terms of bulk density and frequency. Fig. 4.12 represents soil specimens of 1.0 Mg/m^3 with excitation at a frequency of 0.2 Hz, while Figs 4.13 and 4.14 were cases of different frequency and bulk density, respectively. After calculation, the dynamic shear strength parameters can be listed in Table 4.2.

It was deduced that dynamic shear strength in this case was affected by bulk density while significant influence of loading frequency was not found. It was seen that the angles of internal friction were different with different bulk densities. Bulk density of 1.0 Mg/m^3 brought about a higher angle of dynamic internal friction and higher shear strength when compared to one of 0.8 Mg/m^3. In contrast, calculated shear strengths in cases of different frequencies were identical even when there were small differences of angles of dynamic internal friction. Similar results have been recognized in a cyclic axial loading test for transient shear strength of saturated sand by Zhang[97]. He reported that the angle of

dynamic internal friction is not affected by frequency of cyclic stress but it has a nearly linear relationship with bulk density.

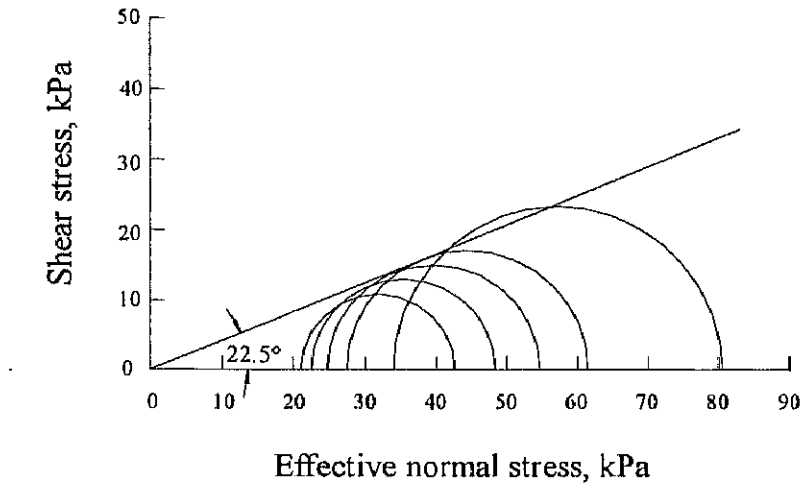

Fig. 4.12 Cyclic torsional shear strength (ρ = 1.0 Mg/m^3, f = 0.2 Hz).

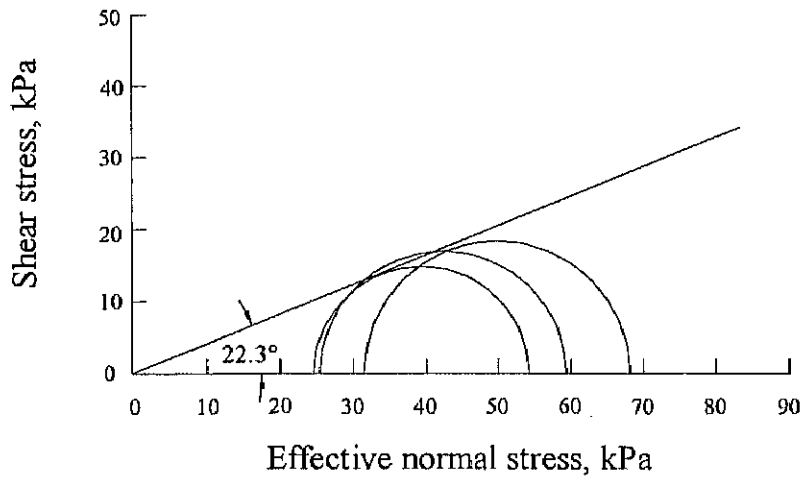

Fig. 4.13 Cyclic torsional shear strength (ρ = 1.0 Mg/m^3, f = 0.5 Hz).

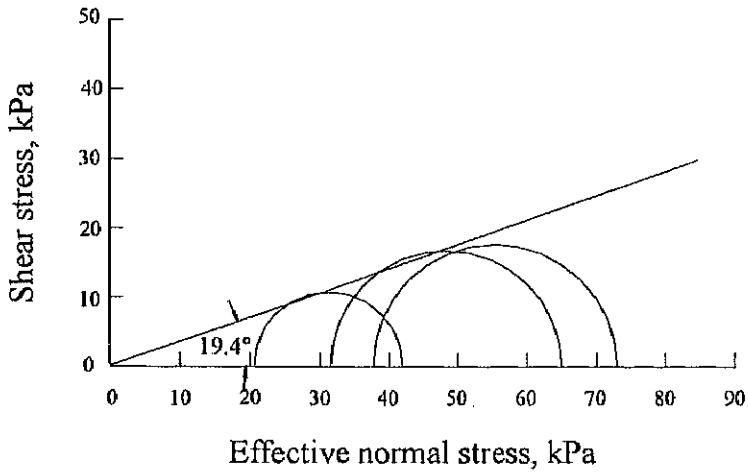

Fig. 4.14 Cyclic torsional shear strength ($\rho = 0.8$ Mg/m^3, $f = 0.2$ Hz).

Table 4.2 Shear strength's parameters with test conditions

Test mode	Frequency, Hz	Bulk density, Mg/m^3	Angle of internal friction, deg.	Strength equation
Cyclic torsional shear loading test	0.2	1.0	22.5	$\tau_{z\theta} = 0.40\sigma'_m$
	0.2	0.8	19.4	$\tau_{z\theta} = 0.35\sigma'_m$
	0.5	1.0	22.3	$\tau_{z\theta} = 0.40\sigma'_m$
Conventional triaxial test		1.0	23.7	$\tau = 0.43\sigma'_m$

Although the comparison between the static and dynamic shear strengths cannot be done directly because of the difference in the definitions, it implied more or less that the specimen under the dynamic condition might have lower effective shear strength against a relevant external force than one under the static condition. This might be mainly due to the insufficient degree of dispersion of pore water pressure within soil specimens. In static

condition of the triaxial test, the loading rate was set to be slow enough to acquire a complete dispersion of pore water pressure in soil. In contrast, in dynamic loading condition, the pore water was excited at a certain loading frequency in which the loading rate was rather high. Consequently, it might have resulted in higher pore water pressure in soil specimens which lowered the effective stress. In this study, the strain rate was set at 0.05 %/min in the triaxial test while this was varied from 3 to 12 %/min in the cyclic torsional shear loading test at the excitation of 0.5 Hz as shown in Fig. 4.15.

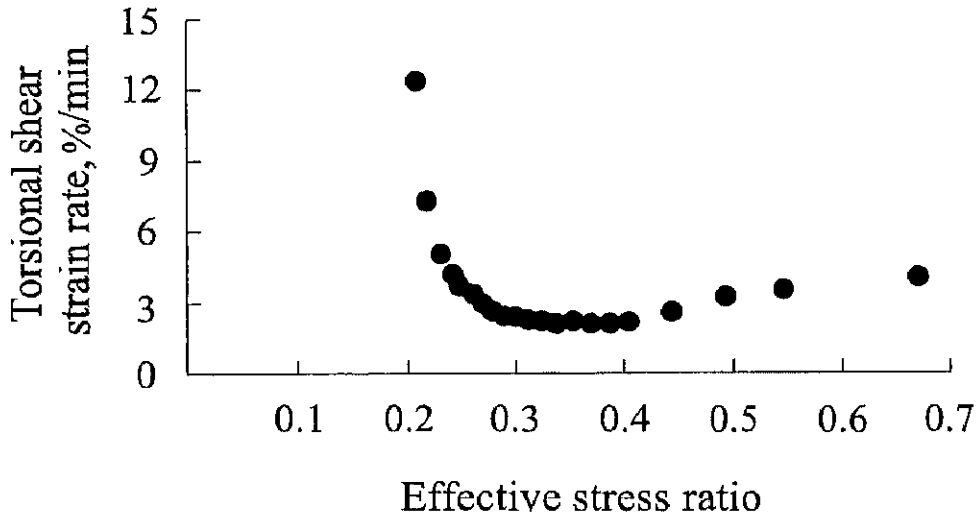

Fig. 4.15 Torsional shear strain rate during experiment
(ρ = 1.0 Mg/m^3, f = 0.5 Hz).

4.3.3 Residual torsional shear strain

Fig. 4.16 illustrates the relationship between the effective stress ratio and the torsional shear stress. This investigation was done in order to clarify the change in soil specimen at any state of effective strain. When the constant amount of cyclic loading has been applied to the soil specimen, not only the corresponding strain but also the effective stress was changed. The state of effective stress can be recognized by the effective stress

ratio. The effective stress ratio was determined by dividing the amplitude of torsional shear stress with the amount of effective confining stress at the end of the loading cycle. Correspondingly, residual torsional shear strain was defined from the double amplitude of torsional shear strain at the end of the loading cycle.

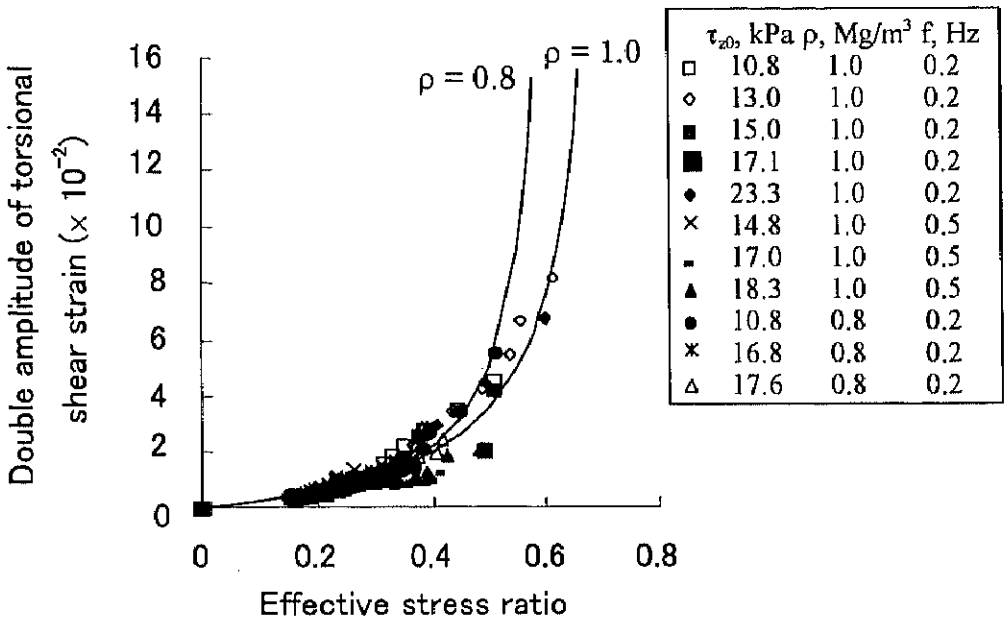

Fig. 4.16 Double amplitude of torsional shear strain versus effective stress ratio.

By virtue of this manipulation, the amount of the strain at any stress state can be manifested. As shown in the figure, there were noteworthy relationships between the residual torsional shear strain and the effective stress ratio for two values of bulk densities. The difference between the results of the two bulk densities was not clear. This may be because the values of the two bulk densities were not so much different and the test number for the bulk density of 0.8 Mg/m^3 was quite small. It is recognized that the loading frequency did not affect this relationship. The relationship between these parameters was first introduced by Hyodo *et al.*[41] and confirmed validly by later research works.[39),40)] It was suggested that the best-fit curve for this relationship was a hyperbola. In this specific

test, the relationship can be described by equations (4.6) and (4.7) for bulk densities of 0.8 and 1.0 Mg/m^3, respectively.

$$\gamma_a = \frac{\eta}{0.050 - 0.080\eta} \qquad 4.6$$

$$\gamma_a = \frac{\eta}{0.045 - 0.062\eta} \qquad 4.7$$

The γ_a is double amplitude of torsional shear strain and η is effective stress ratio. These hyperbolic equations have asymptotes at η = 0.63 and 0.73, respectively. These equations are helpful in determining residual torsional shear strain at specific effective stress ratio.

By adaptation of these equations, the residual torsional shear strain can be calculated. As listed in Table 4.2 the dynamic shear strength can expressed by $\tau_{z0} = 0.35\sigma'_c$ and $\tau_{z0} = 0.40\sigma'_c$ for bulk density of 0.8 and 1.0 Mg/m^3, respectively. Substituting them for values of effective stress ratio to equations (4.6) and (4.7) yielded residual torsional shear strain being equal to 1.59×10^{-2} and 1.62×10^{-2}. These values represented residual shear strain at failure for both bulk densities, respectively.

4.3.4 Critical state behavior

Schofield and Wroth[76] proposed the concept that soil and other granular materials, if continuously distorted until they flow as a frictional fluid, will come into a well-defined critical state. When soil reaches this specific state, large deformation takes place. If this happens in the field during vehicular operation, it might result in more compaction of the soil by successive running devices of a vehicle.

In order to characterize critical state under this specific test, close observation was performed on change of the stress path. The physical change of the stress path in Fig. 4.17 was initiated at point-A. This point was specified with zero torsional shear stress and the magnitude of effective confining stress being applied during the consolidation process.

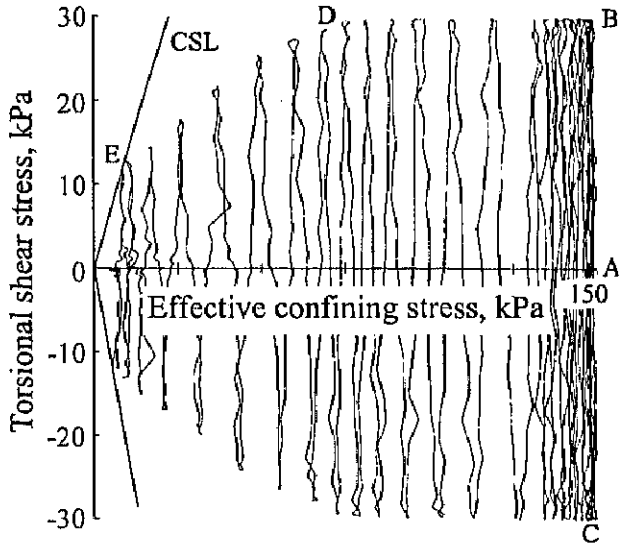

Fig. 4.17 Critical state for cyclic torsional shear loading.

After cyclic excitation began, the stress path rose up to point-B and fell down to point-C. In this way, it continued to fluctuate with the decrease of the effective confining stress until reaching point-D. Afterwards, the stress path moved to zero stress state with the decrease of both the magnitudes of the torsional shear stress and the effective confining stress. According to the critical state theory, the stress path has to encounter critical state at point-E and subsequently might move along the critical state line (CSL) as a frictional flow to the zero state. However, in fact, the test was stopped at point-E due to absence of further shear strength.

To enable quick determination of the critical state under this loading mode, the relationship between effective stress ratio and double amplitude of torsional shear strain in Fig. 4.16 was taken into account. With adaptation of the method proposed by Hyodo *et al.*[41], the critical state can be determined at the asymptote of the hyperbolic relationship of effective stress ratio and double amplitude of torsional shear strain. According to equations

(4.6) and (4.7), since asymptotes can be represented by $\eta = 0.63$ and 0.73, the critical states for bulk density of 0.8 and 1.0 Mg/m^3 under this specific mode can be expressed by $\tau_{z\theta} = 0.63\sigma'_c$ and $\tau_{z\theta} = 0.73\sigma'_c$, respectively. The critical state parameters for this soil in both static and dynamic tests were provided in Table 4.3.

Table 4.3 Critical state's parameters with test conditions

Test mode	Bulk density, Mg/m^3	Critical state equation
Cyclic torsional shear loading test	1.0	$\tau_{z\theta} = 0.73\sigma'_m$
	0.8	$\tau_{z\theta} = 0.63\sigma'_m$
Conventional triaxial test	1.0	$(\sigma'_1-\sigma'_3)/2 = 0.64\sigma'_m$

By applying equations (4.3) and (4.5), the calculation yielded $\tau_{z\theta} = (\sigma'_1-\sigma'_3)/2$. Comparison between critical states in both tests listed in Table 4.3 cannot be done directly because the soil specimens were in different modes of external forces. However, the results in Table 4.3 indicated that soil specimen being under cyclic loading mode might hardly reach critical state when compared to one under static loading mode. This might be caused by some structural change in the soil due to excitation which results in more force being needed to reach critical state.

4.3.5 Nc at failure and some parameters involved

In order to establish a relationship between Nc required at failure and some parameters involved, analyses in Figs. 4.18, 4.19 and 4.20 were carried out. This study is to contribute to understanding the behavior of field soil compaction in terms of numbers of

wheel passes and dynamic load. The Nc required for failure was found to depend on the loading conditions. Fig. 4.18 shows a relationship between the torsional shear stress and Nc, whereas Figs. 4.19 and 4.20 represent relationships between the torsional shear stress versus the pore water pressure, and $Nc \times \tau_{z\theta}$ versus the pore water pressure, respectively. The term $Nc \times \tau_{z\theta}$ served as an indicator of loading intensity. The results shown in these figures were obtained from tests under the loading frequency of 0.2 Hz and bulk density of 1.0 Mg/m^3.

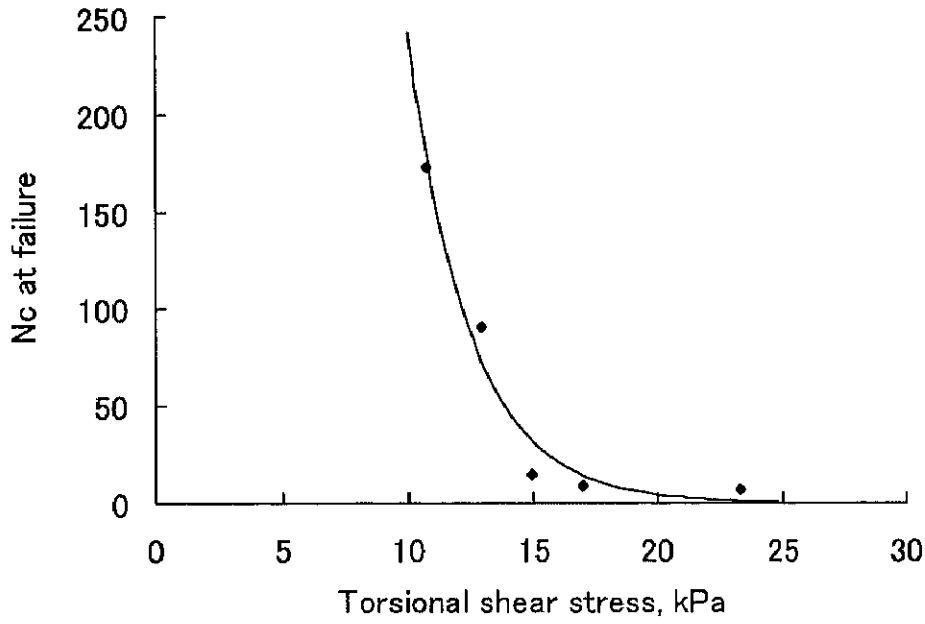

Fig. 4.18 Torsional shear strain versus Nc at failure.

As presented in Fig. 4.18, the decrease of the required Nc was accelerated with the increase of torsional shear stress. It suggested that the significant failure of the soil specimen took place within a certain range of loading magnitude. For instance, this range took about 10 to 24 kPa in Fig. 4.18. Beyond this range, the soil specimen was found to fail on the way of the trace of the first loading cycle. On the other hand, under a lower loading, the soil specimen did not reach failure state even when placing load with a higher Nc.

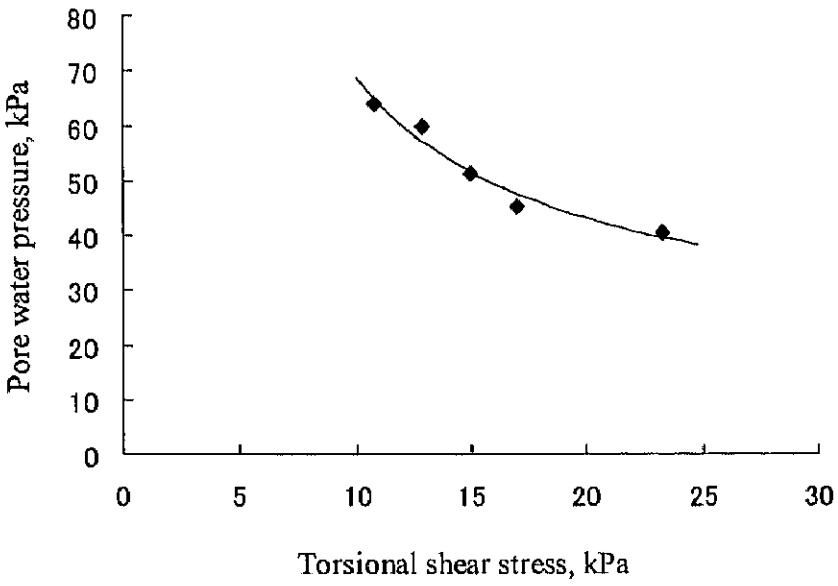

Fig. 4.19 Torsional shear stress versus pore water pressure at failure.

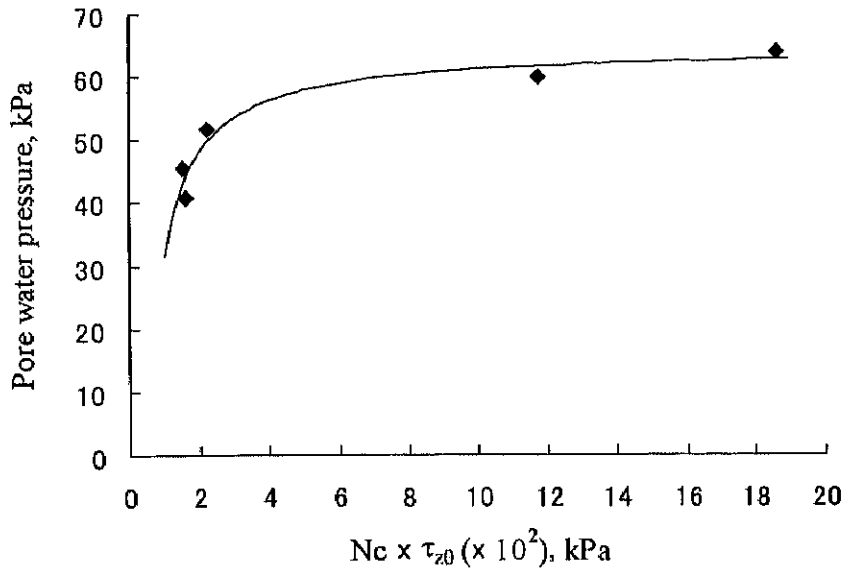

Fig. 4.20 Loading intensity versus pore water pressure at failure.

Based on these results, it can be stated that the soil failure heavily depended on the loading magnitude. However, in this specific range of loading magnitude, the Nc played a major role in leading to soil failure.

Since the strain was found to be constant at failure, as described previously, the pore water pressure may be considered as the main indicator to distinguish the results of different loading conditions. The result in Fig. 4.19 suggested that the loading with a lower magnitude resulted in higher excess pore water pressure at failure when compared to the loading with a higher one. Fig. 4.20 showed that the increase of $Nc \times \tau_{z\theta}$ was followed by the increase of excess pore water pressure. This relationship characterizes the effect of loading intensity on soil failure. It is of interest to note that soil under lower loading intensity failed with small development of pore water pressure. However, this case can be found only for $Nc \times \tau_{z\theta}$ deriving from the combination between high $\tau_{z\theta}$ and low Nc. The results in Figs. 4.19 and 4.20 reflected the cooperation of loading magnitude and Nc in leading to failure of soil; when the loading magnitude is low, the Nc must be high, resulting in high excess pore water pressure so that the stress state meets the failure condition.

4.4 Summary

The failure characteristics of soil under cyclic torsional shear loading were investigated. With consideration of soil-wheel interrelationship, the failure state should be defined based on the maximum shear stress criteria of the classical shear strength theory rather than the large development of soil deformation that is used in earthquake study. The dynamic shear strengths of soil were observed in different loading conditions. Also, a comparative discussion with the static shear strength was made to some extent. The critical

state under this specific loading was clarified with the help of the relationship between effective stress ratio and amplitude of torsional shear strain. This relationship was found to not be affected by loading frequency. Moreover, with adaptation of this relationship, the amount of strain at failure can be recognized. The Nc required for failure and loading magnitude were also observed in an attempt to contribute to understanding the effect of dynamic load and number of wheel passes on the behavior of soil during machinery operation in the field.